Astron. Astrophys. 335, 691–702 (1998)

ASTRONOMY
AND
ASTROPHYSICS

Element fractionation in the solar chromosphere driven by ionization-diffusion processes

Hardi Peter⋆

Max-Planck-Institut für Aeronomie, D-37191 Katlenburg-Lindau, Germany (hpeter@linmpi.mpg.de)

Received 11 August 1997 / Accepted 24 March 1998

Abstract. An ionization-diffusion mechanism is proposed to understand the first ionization potential (FIP) fractionation as observed in the solar corona and the solar wind. The enrichment of the low-FIP elements ($<$10 eV) compared to the high-FIP elements in a large variety of phenomena, as e. g. slow and fast wind or polar plumes, is explained. Also the special behaviour of the heavy noble gases becomes perceptive and the absolute fractionation, i. e. in relation to hydrogen, can be calculated and fits well to the measurements. Additionally the theoretical velocity-dependence of the fractionation will be used to determine the velocities of the solar wind in the chromosphere. The main achievement of this paper is the explanation of a great variety of fractionation-related phenomena on the basis of *one* single model.

Key words: Sun: abundances – Sun: chromosphere – solar wind

1. Introduction

The relative elemental abundances change significantly from the photosphere to the corona and the solar wind: elements with a first ionization potential (FIP) below 10 eV (low-FIP elements) are enriched compared to those with a FIP higher than 10 eV (high-FIP elements). The factor of enhancement is typically of the order of 4 (2) in the slow (fast) solar wind (see Fig. 1). This *fractionation*, also called *FIP-effect*, is found not only from the photosphere to the solar wind, but also from the photosphere to the corona, e. g. in polar plumes. It was already in the Sixties that a change in the abundances from the photosphere to the corona was recognized by Pottasch (1963). Much observational work on both, spectroscopic based diagnostics and in-situ measurements in the solar wind, has been done in the meantime.

The FIP-effect is present not only on the sun, but can also be found with stars. In a series of papers Drake et al. (1995, 1996, 1997) looked for the fractionation in three stars: α-Centauri showing a similar FIP-effect as the sun, ε-Eridani with a smaller fractionation and Procyon, where no FIP-effect could be found. This leads to the question why some stars show a fractionation and others do not, which will be briefly discussed in the conclusions.

It is of importance to understand the abundance variations from the solar or stellar surface to the corona/wind for a number of reasons. The abundances are crucial for the diagnosis of the coronal spectra such as emission measure analysis and density or temperature diagnostics using line ratio techniques. The densities of the minor species are also important for the thermodynamics of the corona, because they dominate the radiative losses at temperatures above $\approx 5 \cdot 10^4$ K (e. g. Cook et al. 1989). Furthermore the chemical composition of the solar (stellar) wind is of importance for mapping back the source region of the wind — only those parts of the chromosphere/corona can contribute a significant fraction of the mass flux to the wind that have abundances which are similar to those in the wind (see e. g. Geiss et al. 1995).

Results of fractionation models might be used to determine atmospheric parameters; e. g. in the present model the velocities of the slow and fast wind in the chromosphere can be calculated by comparing the fractionation in the wind with the model results for the chromosphere. But it may also be possible (in future models) to get information on the heating mechanisms or the magnetic topology by using the elemental abundances. Thus the theoretical understanding of the fractionation may lead to new diagnostic techniques for the chromosphere and the corona.

Many attempts have been made to understand the fractionation theoretically. See Hénoux & Somov (1992), Meyer (1993), Hénoux (1995) or von Steiger et al. (1997) for an overview. It is now widely accepted that the ion-neutral-separation is the most relevant process leading to the fractionation, located in the chromosphere, at temperatures below 10^4 K (see Sect. 2.5): the step between the two plateaus is at 10 eV, (see Fig. 1) which corresponds to the energy of the Lyman-α line (1215 Å), the most prominent line in the UV. As Lyman-α can ionize the low- but not the high-FIPs, the photoionization and thus the separation of the ions from the neutrals must be expected to play an important role. Various scenarios were presented, but the model of von Steiger & Geiss (1989) was the first which allowed a detailed comparison of its predictions with the measurements of the fractionation in the solar energetic particles (SEP) and in the slow solar wind.

⋆ *Present address:* High Altitude Observatory/NCAR, P.O. Box 3000, Boulder, CO 80307-3000, USA

Recently Vauclair (1996) presented an interesting preliminary model with a completely different idea: horizontal magnetic field emerging from the photosphere is lifting the ions but not the neutrals. This would enrich those elements in the corona that are easy to ionize: the low-FIP elements. The main problem of this model is that it is restricted to regions with predominately horizontal magnetic fields. Thus one cannot expect an explanation for the polar plumes or the fast wind coming out of the coronal funnels.

The present paper will follow the "tradition" of the von Steiger & Geiss (1989) model. Their main idea was to combine the effects of photoionization and diffusion to describe an ion-neutral-separation. In their model the pressure gradient drives an initially neutral mixture *across* ambient magnetic structures. Marsch et al. (1995) applied the same process for a stationary flow *along* the magnetic field lines. They found a very simple formula describing the fractionation in the slow wind: the fractionation is proportional to the square root of the quotients of the respective ionization times and collision frequencies in the neutral phase. Following the philosophy of the Marsch et al. (1995) model, Peter (1996) presented an analytical study leading to a velocity-dependence of the fractionation. This enabled the explanation of the fractionation not only in the slow, but also in the fast wind within the same model.

In the present paper the analysis of Peter (1996) will be extended to explain a greater variety of fractionation phenomena summarized in Sect. 2. Some simple ideas to understand the fractionation mechanisms are presented in Sect. 3. A more detailed discussion and a comparison to measurements of the velocity-dependence as found by Peter (1996) will be presented in Sect. 5.1, as it was *not* done in the original paper. Applying his results to the heavy noble gases their fractionation can be understood qualitatively (Sect. 5.2). For a description of the absolute fractionation or the strong enrichments of magnesium in polar plumes numerical trace gas models have to be applied (Sect. 5.3 and 5.4). The respective numerical calculations for the hydrogen background have been done by Peter & Marsch (1998). In Sect. 6 the role the of diffusion for the fractionation will be discussed in more detail. Finally Sect. 7 summarizes the main results of this paper.

2. Observational constraints

The fractionation compares the relative abundance of an element j in relation to another element k in the solar wind (SW) or the corona with the respective value in the photosphere. It is defined as

$$f_{j,k} := \frac{(N_j/N_k)^{\mathrm{SW/corona}}}{(N_j/N_k)^{\mathrm{photosphere}}}. \quad (1)$$

Especially for the in-situ measurements in the solar wind the fractionation is mostly taken in relation to the typical high-FIP element oxygen. This is because O is the third abundant element (after H and He) in the solar atmosphere and wind.

The abundances in the solar photosphere can be found e. g. in the work of Anders & Grevesse (1989). These values are quite well known. But it is harder to determine the abundances in the corona: there the densities have to be deduced by more or less problematic UV-diagnostic techniques, e. g. line ratio or emission-measure analysis. Much more reliable are the in-situ measurements in the solar wind. But in both cases it is hard to determine the absolute abundances, i. e. the values in relation to hydrogen. In the corona absolute abundances have to be determined by the complicated line to continuum ratio techniques because of the absence of hydrogen lines. In the solar wind the enormous difference in the densities of hydrogen and the trace gases, and thus of the respective count rates, causes huge technical problems; e. g. in the time one oxygen particle is measured about 1200 protons will be found.

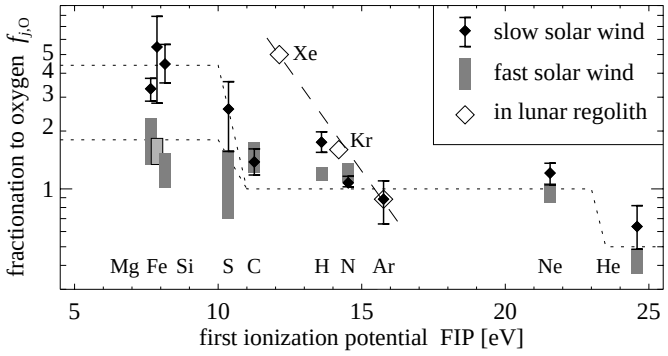

Fig. 1. Measured fractionation in the solar wind in relation to oxygen. The dotted lines should only indicate the measured high- and low-FIP plateaus for the slow and fast wind respectively (they are not a fit to the data). The heavy noble gases (Xe, Kr, Ar) form their "own line" (dashed). Helium plays a special role and forms its own "plateau". The measurements in lunar regolith reflect the abundances in the slow wind (see text). The fractionation of O in relation to O is, by definition, one. For this the data points for O are omitted.

The most relevant observational constraints are collected in Fig. 1, showing the fractionation from the photosphere to the solar wind as given by different references: The in-situ measurements in the slow and fast wind are represented by the bars and rectangles respectively (from the collection of von Steiger et al. 1995). The high- and low-FIP plateaus are indicated by the dotted lines (see Sect. 2.1). The open diamonds show the relative abundances as obtained from lunar regolith for the heavy noble gases (Wieler & Baur 1995; see Sect. 2.3).

A more detailed discussion of the measurements of the fractionation in a great variety of coronal and solar wind structures, e. g. of hot and cool loops, can be found in the review article of Meyer (1996).

2.1. Two-plateau-structure and velocity-dependence

First of all there are two clearly distinguishable plateaus, one for the low-FIPs and one for the high-FIPs, in the slow as well as in the high speed solar wind.

This two-plateau-structure becomes even clearer in measurements of solar energetic particles (e. g. Anders & Grevesse 1989, their Fig. 3), where more elements are observable. The

dotted lines in Fig. 1 should only indicate the location of the two plateaus (they are not a fit to the measurements). The step-height between the two plateaus is a factor of four in the slow, a factor of two in the fast wind. Just recently Raymond et al. (1997) presented spectroscopic measurements of UVCS on SOHO also showing this structure in streamers (see below).

Another important feature, which is not shown in Fig. 1, is the result of e. g. Widing & Feldman (1992) or recently Sheeley (1996). They found a very strong fractionation of Mg to Ne of the order of 10 (!) in polar plumes. And they conclude that these plumes have to be quasi-static; because of their strong abundance anomalies they cannot contribute to the solar wind.

This leads to a velocity-dependence of the fractionation: in the quasi-static plumes the fractionation is stronger than in the slow wind, while the separation is weakest in the fast wind. Additionally Bochsler et al. (1996) reported that in some high-velocity streams no fractionation was found.

2.2. Absolute fractionation

As hydrogen is the most abundant element it is of importance to know the fractionation in relation to hydrogen, i. e. the absolute fractionation. This is the key to find out which elements are absolutely enriched and which are depleted.

Following von Steiger et al. (1995) the fractionation of hydrogen to oxygen is of the order of 2 in the slow and a factor of 1.2 in the fast wind. Thus the high-FIPs are absolutely depleted in the slow wind, while their absolute abundance remains nearly unchanged in the fast wind. As pointed out in the review of Meyer (1996) there are many other results for coronal measurements, derived from spectroscopic diagnostics. E.g. recently Raymond et al. (1997) found a fractionation of H to O corresponding to the slow wind measurements of von Steiger et al. (1995) in active region streamers and the legs of quiescent helmet streamers. This paper will concentrate on the more reliable values of the in-situ measurements of von Steiger et al (1995), see above.

2.3. Heavy noble gases

Plotting the fractionation versus the FIP, the noble gases form their "own line" (see Fig. 1) Because of their very low abundance the noble gases Xe and Kr cannot be measured in the corona or in-situ in the solar wind. But as the solar wind hits the moon directly, some of the solar wind particles can be implanted into the lunar material. The non-volatile elements, i. e. the noble gases, can remain in the material without a significant change of their abundances over a long period. Wieler & Baur (1995) took advantage of this effect and determined the abundances of Xe, Kr and Ar from samples of lunar regolith. As the moon is (more or less) in the ecliptic plane, their results should reflect the conditions in the slow wind. It should be noted that Wieler & Bauer have found that the fractionation in the older samples (1-3$\cdot 10^9$ years) is about 30% stronger than in the younger ones ($< 10^8$ years).

2.4. Helium

Helium shows a somewhat strange behaviour: in the "quiet" solar wind it is depleted compared to the other high-FIPs by a factor of up to two (see Fig. 1), but it can also be strongly enriched, e. g. in the driver gas of flare-induced interplanetary shocks (e. g. Hirschberg et al. 1970). As shown by Peter & Marsch (1998) these effects cannot be understood by the same processes leading to the fractionation of the minor species, as presented in this paper. This negative result is not surprising as helium is not a minor element.

But the changes in the abundance of helium can be understood in a coronal/solar wind model, where also effects like the thermal force in the transition region are taken into account (see Hansteen et al. 1997).

2.5. Location of the relevant processes and geometry

The fact that an ion-neutral separation is used to describe the fractionation restricts the possible locations of the fractionation processes to regions where neutrals *and* ions are present, i. e. where the first ionization takes place. Applied to the solar atmosphere this is the region well above the temperature minimum and below 10^4 K. Because of the short ionization-diffusion times, this fractionation layer is thin (see e. g. Marsch et al. 1995). For typical velocities of the solar wind in its source region of 500 m/s (see below) and ionization times of 1 to 100 s, the ionization layer has a thickness of up to only 50 km. In the paper of Peter & Marsch (1998), describing the background models for the here presented fractionation models, a detailed description of this region can be found.

Concerning the source region of the *fast wind* the material is assumed to flow out of the coronal funnels. Mapping back the measured particle flux at 1 AU to the base region of a funnel the resulting velocity is of the order of 500 m/s (see Peter & Marsch 1998 for a more detailed description). The fractionation processes are located at chromospheric low temperature regions at the base of the funnels. Above the fractionation layer, where the material is ionized, the trace gases are trapped by the proton background and are transported into the solar wind. Through the transition region and the corona the abundances remain unchanged, because the very efficient Coulomb-coupling renders equal velocities for all species, which prevents any further fractionation (compare Sect. 6.2). Thus the fractionation in the chromosphere as described by the presented model is comparable to the measurements in the solar wind.

In the case of the *slow wind* the situation is a bit different. A possible scenario, supported by recent SOHO observations (see Sheeley et al. 1997), is as follows. The loops are fed by a flow at their footpoints, which are located in the chromosphere. In a thin layer at below 10^4 K (see above) at the footpoints of the loops the material gets fractionated; thus fractionated material is accumulated in the loops. After some time the loops open and the fractionated material escapes forming the slow wind. In this scenario, the fractionated material is accumulated in the loops leading to a higher pressure, which is trying to stop the flow.

But the aim of this paper is not to establish a loop model — this scenario should be taken just as an idea.

Another possibility for the loop situation is a kind of "siphon flow" through the loop (e.g. Cargill & Priest 1980). Klimchuk & Mariska (1988), who modeled heating related flows in loops, found velocities at the foot point regions of a loop of the order of 0.3 km/s (see their Fig. 2) — an up-flow in the one, a down-flow in the other footpoint. This velocity is a bit lower than the the velocities at the base of the funnels as mentioned above.

As it can be seen from (5), the sign of the velocity does not play a role for the fractionation, which means that only the transit time through the ionization-diffusion layer is of importance and not the direction of the flow (see Sect. 3). For this in an up-flowing as well as in a down-flowing region (i.e. in two foot points of a loop with a siphon flow) the material in the ionized region becomes fractionated. This means that a siphon flow through a loop may well cause an enrichment of the low-FIPs in the loop.

Concerning the geometry, the footpoint region of a loop is comparable to the base of a coronal funnel: in both cases the magnetic field is more or less vertical and a one-dimensional model (along the field lines) can be applied. Thus a one-dimensional multi-fluid model for a chromospheric region at below 10^4 K will be considered to describe the fractionation of the elements.

3. Basic fractionation mechanisms

The rates for (electron) collisional ionization at temperatures of 10^4 K, as found in the fractionation layer, are small compared to the photoionization rates; e.g. for hydrogen the respective rates are $7.8{\cdot}10^{-5}\,\mathrm{s}^{-1}$ (Lotz 1967) and $1.4{\cdot}10^{-2}\,\mathrm{s}^{-1}$ (von Steiger & Geiss 1989). Thus only the photoionization can be expected to have a significant impact on the fractionation. Following the Marsch et al. (1995) model the ionizing UV radiation is coming from the above layers of the upper chromosphere and transition region. As the chromosphere is more or less optically thin in the EUV (except for some lines like e.g. Lyα) the ionization rates are approximately constant with depth for the minor species.

In Fig. 2 (left) the basic fractionation mechanisms are illustrated:

The *ionization* of the material is the main process that causes the fractionation. The low-FIPs have short ionization times and are coupled quickly to the solar wind flow of the main gas, ionized hydrogen. The high-FIPs with their longer ionization times are harder to ionize: for this, they remain longer in the neutral phase and are coupled later to the solar wind than the low-FIPs. Thus the low-FIPs are preferably transported out of the chromosphere into the interplanetary space. This simple picture renders the enrichment of the low-FIPs understandable.

As well the *diffusion* in the neutral phase plays an important role. At the top of the ionization layer, where the material is ionized, the very effective Coulomb-coupling causes equal velocities of the different species. But at the bottom of the layer, in the neutral phase, the collisions are less effective: neutral-neutral as well as neutral-ion collisions are about a factor of 1000 less effective than the ion-ion interaction (see Table 2). For this a diffusion at the bottom of the layer is possible (see also Sect. 6.2 for a more quantitative discussion). This diffusion regulates the fractionation simply by regulating the velocity differences of the trace gases. It should be kept in mind that even if the diffusive velocities are small, the influence on the fractionation could be non-negligible: following (7), the quotient of the diffusion velocities is of importance, which can be large, even if the absolute values of the diffusion velocities are small.

At last the combination of ionization and diffusion leads to the two-plateau structure of the fractionation as shown in Fig. 1. Quantitatively speaking the combination of *atomic* parameters, namely the cross sections for photoionization and elastic collisions, forms the two plateaus, see (7). Thus the presented model is independent of the assumptions concerning e.g. the structure of the magnetic field topology: the results of the model can be used for the explanation of the fractionation in a wide variety of solar structures, like coronal funnels, loops or polar plumes.

But there is yet a third mechanism, leading to a *velocity-dependence* of the fractionation. If the transit time through the ionization layer is shorter, the fractionation will be weaker than for a longer transit time, because the above described processes have less time to act. As shorter transit times mean higher velocities, this implies that the fractionation is weaker for higher velocities. This mechanism, first pointed out by Peter (1996), is reflected in (5) below. But this discussion also clarifies that the fractionation depends only on the absolute value of the velocity (which corresponds to the transit time), but *not* to the direction of the flow!

It is helpful to look at the analogy between the fractionation processes in the solar chromosphere and the evaporation of different kinds of perfumes which are dissolved in a bathing tub (see right of Fig. 2, following an idea of R. Bodmer). If the water is heated, buoyancy will drive a flow of steam; this is the analogy to the solar wind. The heating lamp, which causes the evaporation of the perfumes, compares to the ionizing UV radiation. The volatile kinds of perfume have a shorter "evaporation time" (corresponding to the ionization time); for this they will be enriched in the steam above the tub. But as in the solar chromosphere the diffusion also regulates the fractionation: the enrichment of the volatile elements is regulated by their ability to diffuse through the background of water.

In this bathing tub analogy it is immediately perceptive that the abundances in the water (the photosphere) do not have to be the same as in the steam above the tub (the corona) and thus a fractionation is present. The ionization-diffusion layer in the solar chromosphere as described in the present paper compares to the (thin) layer under the water surface.

The thickness of the ionization-diffusion layer on the Sun can be estimated by using the typical flow speed of 500 m/s and the ionization time, which is roughly speaking of the order of 10 s (see Table 1), leading to some km. This means that the "natural" length scale for the fractionation processes as proposed in the present paper is very small and the ion-neutral separation takes place in a very thin layer.

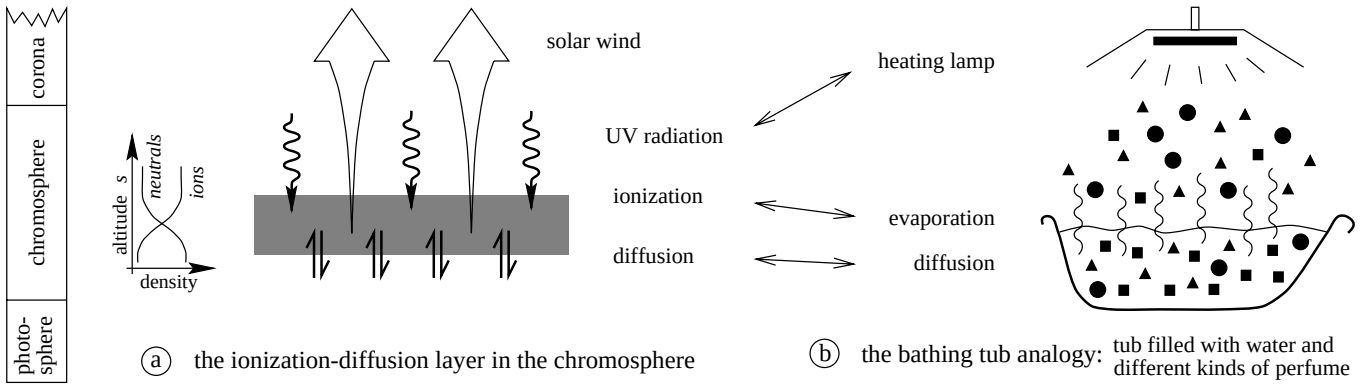

Fig. 2. Basic fractionation mechanisms and the "bathing tub analogy" following an idea of R. Bodmer.

This is finally the reason, why the recombination is not of great importance. Because of the long recombination times of typically 200 s (see Table. 1, $1/\gamma_{\rm rec}$), the length scale of recombination is of the order of some 100 km. Even though this is much smaller than the length scale of the objects in mind (coronal funnels or loops, see Sect. 2.5), it is much larger than the thickness of the ionization layer where the fractionation takes place. In fact it turns out that the numerical models including recombination as discussed in Sect. 5.3, give results comparable to the analytic studies in Sect. 5.1, where recombination is neglected.

Also an other mechanism can be present, especially if a coronal loop is considered: fractionation due to diffusion perpendicular to the magnetic field as described by von Steiger & Geiss (1989). In their (time-dependent) calculations they need up to 100 s to reach the fractionation as observed in the slow wind (see their Figs. 2 and 3). As the thickness of the ionization-diffusion layer, where the present model operates, is only of the order of some km (see above), the transit time is shorter than the fractionation time of von Steiger & Geiss (1989). For this no strong additional effect can be expected by the diffusion perpendicular to the magnetic field — nevertheless it should be included in future models.

4. Model ingredients

4.1. Multi-fluid transport equations

For the description of the fractionation for every trace gas a set of transport equations (see e. g. Schunk 1975) has to be solved. Here the same formulation as in the background model of Peter & Marsch (1998) will be used. The equations of continuity and momentum for a species j for a one-dimensional case along the coordinate s parallel to the magnetic field and for a single temperature read

$$(n_j\,u_j)' \;=\; \sum_{j'} \big(\gamma_{j'\,j}\,n_{j'} - \gamma_{jj'}\,n_j\big), \tag{2}$$

$$\begin{aligned} u_j\,u_j' \;+\; \frac{1}{n_j}\,(v_j^2\,n_j)' \;+\; \frac{Z_j}{n_{\rm e}}\,(v_j^2\,n_{\rm e})' \;+\; g \;=\; \\ -\sum_k \nu_{jk}\,(u_j - u_k) \;-\; \sum_{j'} \frac{n_{j'}}{n_j}\gamma_{j'\,j}\,(u_j - u_{j'}). \end{aligned} \tag{3}$$

Here n_j and u_j are the particle density and the s-component of the velocity of the species j. The prime, $'$, denotes the derivative with respect to s. The sources and sinks for the particle flux density $n_j\,u_j$ are due to ionization and recombination with the respective rates $\gamma_{j'\,j}$. The sound speed is given by $v_j = (k_{\rm B}T/m_j)^{1/2}$, with Boltzmann's constant $k_{\rm B}$, temperature T and atomic mass m. Z_j denotes the charge number of the species j, and g is the gravitational acceleration (pointing to the negative s-direction). The exchange of momentum between the species is due to ionization/recombination and elastic collisions with the respective rates $\gamma_{j'\,j}$ and ν_{jk}. The latter ones obey $m_j\,n_j\,\nu_{jk} = m_k\,n_k\,\nu_{kj}$.

Only collisions of the respective trace gas (neutral and ionized components) with the background, i. e. hydrogen, are considered, while the interaction between the different trace gases is neglected: every trace gas is treated as a collection of test particles.

In the case of the trace gases, no energy equation has to be solved because the thermodynamics were solved together with the main gas (see Peter & Marsch 1998).

As in the case of the background model of Peter & Marsch (1998) the ionization rate is assumed to decay as $\gamma'_{\rm ion} = \overline{\sigma}\gamma_{\rm ion}n_n$, where $\overline{\sigma}$ is the (mean) ionization cross section and n_n the density of the neutrals. But one should keep in mind that the ionization rate for the minor elements is nearly constant, which is because of their low abundance.

That the radiation in the wavelength bands, which are relevant for the ionization of the minors, is nearly constant, can also be seen from the work of Vernazza et al. (1981), their Fig. 36. Their (static) semi-empirical radiative transport model includes also the radiation from the under-laying photosphere and lower chromosphere. Thus the present assumption that the radiation field and thus the ionization rate are more or less constant with altitude can at least be funded by their radiative transport model.

To solve the equations numerically, routines of the NAG library were used, as described in the background model of Peter & Marsch (1998).

4.2. Boundary conditions

For the numerical studies (in Sect. 5.3 and 5.4)

The velocities of the neutral and ionized component are assumed to be equal at the top as well as at the bottom of the layer. This is motivated by the fact, that at the bottom the material is mostly neutral, at the top mostly ionized. Thus ionization and recombination cause the components to have the same speed.

At the bottom of the ionization-diffusion layer the abundance of an element and its degree of ionization (following the Saha equilibrium) are given. Finally the ionization rate at the top is set to the value as calculated by von Steiger & Geiss (1989), see their Table 2. These are reprinted in Table 1.

It should be noted, that no absolute value of the velocity or any diffusion velocity between two elements is presumed. The diffusion at the bottom of the ionization-diffusion layer results from the model (see Sect. 6.2).

For the analytical studies (in Sect. 5.1 and 5.2)

For the analytical model, which follows Peter (1996), the following boundary conditions are chosen: all the material at the bottom is neutral, i. e. the density and the flux of the ions vanishes at the bottom. This is different from the boundary conditions for the numerical models as discussed above. In a way this is a stronger version of the above conditions, where the degree of ionization (non-zero above) is forced to be zero at the bottom.

Because the ionization rate is assumed to be constant in the analytical studies, there is no boundary condition needed for the ionization rate.

To solve for the fractionation Peter (1996) made an assumption, which can be considered as an additional boundary condition. This is one of the most critical points in that paper. It is assumed that there is no acceleration for the neutrals at the bottom, $u_n'(0) = 0$. This ad hoc assumption seems reasonable from a physical point of view — why should the neutrals be accelerated at the bottom?

But as every stationary model is determined largely by the given boundary conditions, this assumption has to be proven critically. This can be done with the numerical studies presented in Sect. 5.3, where no assumption was made on the value of the velocity or the acceleration at the bottom (compare above). As an example of a trace gas in the right panel of Fig. 7 the scaled absolute velocity $u_{\rm O}$ of neutral oxygen as resulting from the numerical model is shown (see also Sect. 6.1).

The effect of the gravitational stratification leads to a velocity increasing with altitude (see Peter & Marsch 1998, their Sect. 5). To eliminate this, $u_{\rm O}$ is scaled by the normalized total oxygen density, $\widehat{N}_{\rm O} = [n_{\rm O} + n_{\rm O^+}]/[n_{\rm O}(0) + n_{\rm O^+}(0)]$. The results as shown in Fig. 7 prove that the gradient of the velocity of the neutrals is in-deed small at the bottom, i. e. that the neutrals are flowing "smoothly" into the considered layer.

The numerical studies of the present paper, which are using much "weaker" boundary conditions, justify the critical assumption $u_n'(0) = 0$ in the work of Peter (1996) and in the analytical studies in the present paper.

Table 1. Atomic data.

	A_t	$\log\mathcal{A}$ (photo.)	FIP [eV]	τ [s]	$r_{n\rm H}$ [Å]	α [Å^3]	$\gamma_{\rm rec}/n_{\rm e,16}$ [10^{-3} s^{-1}]	$w_t^\dagger$ [m/s]
H	1	12.00	13.60	65	—	0.667	4.3	—
He	4	10.99	24.59	227	1.56	0.205	4.3	83
C	12	8.56	11.26	27	2.34	1.76	4.7	154
N	14	8.05	14.53	68	2.11	1.10	4.1	108
O	16	8.93	13.62	62	2.26	0.802	3.1	105
Ne	20	8.09	21.56	81	1.75	0.396	2.2	118
Mg	24	7.58	7.65	0.78	3.09	10.6	1.4	681
Si	28	7.55	8.15	1.1	2.91	5.38	5.9	608
S	32	7.21	10.36	11.6	2.58	2.90	4.1	211
Ar	36	6.56	15.76	50	2.07	1.64	3.8	127
K	39	5.12	4.34	0.43	4.22	43.4		669
Ca	40	6.36	6.11	0.70	3.64	22.8	1.1	608
Ti	48	4.99	6.82	0.44	3.39	14.6		823
Fe	56	7.67	7.87	0.91	3.09	8.4	1.4	627
Zn	64	4.60	9.39	2.6	2.98	7.1		385
Kr	84	3.23*	14.00	20.3	2.17	2.48		189
Xe	132	2.23*	12.13	10.1	2.35	4.04		247

*meteoric abundances †for T=10^4 K and $N_{\rm H}$=$4{\cdot}10^{16}$ m^{-3}

4.3. Atomic data

In Table 1 the used atomic data as collected from different references are shown. For every element the atomic mass A_t, the photospheric abundance in a logarithmic scale $\log\mathcal{A}$, the first ionization potential FIP, the ionization time τ, the sum of radii of the colliding particles in the neutral phase $r_{n\rm H}$ (at 10^4 K), the atomic polarizability α, the recombination rate $\gamma_{\rm rec}$ (at 10^4 K) and the ionization diffusion speed w_t as calculated from (6) for 10^4 K and $N_{\rm H}$=$4{\cdot}10^{16}$ m^{-3} are given. The abundances are taken from Anders & Grevesse (1989) and are defined as $\log\mathcal{A}_t := 12 + \log(N_t/N_{\rm H})$, where N_t is the total particle density of the respective trace gas and $N_{\rm H}$ the one of hydrogen. τ, $r_{n\rm H}$ and α are taken from von Steiger & Geiss (1989) and Marsch et al. (1995), $\gamma_{\rm rec}$ from Landini & Monsignori Fossi (1990). Both, $r_{n\rm H}$ and $\gamma_{\rm rec}$ depend weakly on temperature; see the above references for more details. The ionization rates are given by the inverse ionization times, $\gamma_{\rm ion} = 1/\tau$.

In Table 2 the elastic collision frequencies ν_{jk} for a trace gas in a hydrogen background are collected. The values are taken from von Steiger & Geiss (1989). Z_i denotes the charge number and A, α_n and $r_{n\rm H}$ are as given in Table 1.

In both tables T_4 and $n_{?,16}$ are the temperature in 10^4 K and the density in 10^{16} m^{-3} respectively.

Special care has to be taken in the case of oxygen: because O and H have nearly the same first ionization potential the charge exchange between both is very efficient. Follow-

Table 2. Elastic collision frequencies ν_{jk} of the minor species.

j	k	$\nu_{jk}/n_{k,16}$ [s^{-1}]	interaction
n	H	$6.09\,(r_{n\mathrm{H}}\,[\text{Å}])^2\,\big(A_n(A_n+1)\big)^{-1/2}\,T_4^{1/2}$	hard spheres
i	H	$21\,Z_i\big(A_i(A_i+1)\big)^{-1/2}$	induced dipole
n	p	$26\,(\alpha_n\,[\text{Å}^3])^{1/2}\,\big(A_n(A_n+1)\big)^{-1/2}$	induced dipole
i	p	$1.1{\cdot}10^4\,Z_i^2\,\big(A_i(A_i+1)\big)^{-1/2}\,T_4^{-3/2}$	Coulomb

ing Arnaud & Rothenflug (1985) the ionization and recombination rate for oxygen due to this process is given at 10^4 K by $\gamma_{\mathrm{O\,O^+}}/n_{\mathrm{p},16} = 9.1\,\mathrm{s}^{-1}$ and $\gamma_{\mathrm{O^+\,O}}/n_{\mathrm{H},16} = 10\,\mathrm{s}^{-1}$. Both rates depend slightly on the temperature (see the original paper). This process is some orders of magnitude more efficient than the photoionization (compare Table 1).

5. Results

5.1. Velocity-dependent fractionation: slow and fast wind

By simplifying Eqs. (2) and (3) Peter (1996) found a simple formula describing the velocity-dependent fractionation. To achieve this, gravity and recombination were neglected (compare the ionization rate $\gamma_{\mathrm{ion}} = 1/\tau_t$ with γ_{rec} in Table 1). Furthermore he assumed a subsonic flow and the interaction between the neutral and the ionized component of the trace gas to be small compared to the effects of the collisions with the main gas.

Using the boundary conditions as discussed in the second part of Sect. 4.2, one can solve for the total flux $\Phi_t = n_n u_n + n_i u_i$ of a trace gas t,

$$\Phi_t/N_t^\circ \;=\; U_{\mathrm{H}}/2 \pm \sqrt{(U_{\mathrm{H}}/2)^2 + w_t}, \tag{4}$$

where N_t° is the total trace gas density at the bottom. U_{H} denotes the (mean) main gas velocity and $w_t{>}0$ is the ionization-diffusion speed as defined below in (6).

In an up-streaming situation ($U_{\mathrm{H}}{>}0$) only the "+"-sign gives a physical solution, because otherwise the main and the trace gas would flow in opposite directions. For the same reason in a down-streaming situation ($U_{\mathrm{H}}{<}0$) only the "−"-sign is allowed. Within the above approximations it follows from (4) that all the trace gases are faster than the main gas, $|\Phi_t|/N_t^\circ > |U_{\mathrm{H}}|$. As the interest is here only on the trace gases and not on the absolute fractionation, this will be discussed in more detail in Sect. 6.1.

At the top of the layer the material is fully ionized: due to the effective Coulomb-collisions the species have equal velocities there. For this the fractionation (1) can be written as the quotient of the (constant) total fluxes and the total densities at the bottom of two trace gases, $f_{i,j} = (\Phi_i/N_i^\circ)/(\Phi_j/N_j^\circ)$, see Peter (1996). It is easy to show that in an up- as well as in a down-streaming situation the above considerations lead to a fractionation given by

$$f_{j,k} \;=\; \frac{1+\sqrt{1+4(w_j/U_{\mathrm{H}})^2}}{1+\sqrt{1+4(w_k/U_{\mathrm{H}})^2}}. \tag{5}$$

The most important factor entering this formula is the *ionization-diffusion speed* w_j of the respective elements, defined as

$$w_j \;:=\; \frac{v_j}{\sqrt{\tau_j\,\widetilde{\nu}_{j\mathrm{H}}}}, \tag{6}$$

where $\widetilde{\nu}_{j\mathrm{H}}$ is the (reduced) collision frequency between the neutrals of the species j and neutral hydrogen. Generally it is defined as $\widetilde{\nu}_{jk} = \nu_{jk}\,N_{\mathrm{H}}/n_k$. By definition w_j is always positive. The speeds w_j are listed for a number of elements in Table 1.

In the case of small main gas velocities the fractionation following (5) is simply given by the quotient of the respective ionization diffusion speeds, as already calculated by Marsch et al. (1995).

As a rough estimate, the photon flux in the UV can be assumed to be constant, which results in the quotient of the ionization rates, $\gamma_{\mathrm{ion}} = 1/\tau$, to be given by the quotient of the respective ionization cross sections, $\sigma^{(\mathrm{ion})}$. As can be seen from Table 2 the quotient of the collision frequencies depends only weak on the masses of the respective elements and is mainly given by $\widetilde{\nu}_{j\mathrm{H}}/\widetilde{\nu}_{k\mathrm{H}} \approx r_{j\mathrm{H}}^2/r_{k\mathrm{H}}^2$, where $r_{j\mathrm{H}}^2$ can be interpreted as the cross section for the elastic collisions, $\sigma_j^{(\mathrm{coll})}$.

Thus the fractionation in the case of small velocities can be written as

$$f_{j,k} \;=\; \frac{w_j}{w_k} \approx \sqrt{\frac{\tau_k}{\tau_j}\,\frac{\widetilde{\nu}_{k\mathrm{H}}}{\widetilde{\nu}_{j\mathrm{H}}}} \;\approx\; \left(\frac{\sigma_j^{(\mathrm{ion})}}{\sigma_k^{(\mathrm{ion})}}\,\frac{\sigma_k^{(\mathrm{coll})}}{\sigma_j^{(\mathrm{coll})}}\right)^{1/2}. \tag{7}$$

This clearly shows that the processes of photoionization (τ) and diffusion ($\widetilde{\nu}$) are most relevant and that the fractionation is basically given by *atomic* parameters, namely the cross sections for photoionization and elastic collisions. It does not depend on the assumed geometry of the considered region (see also Sect. 3).

But as can be seen from (5) the result of Peter (1996) goes much further: it also includes a dependence on the main gas velocity in the chromosphere and can thus reproduce the fractionation not only in the slow wind, but also in the fast wind. As it was *not* done by Peter (1996) this velocity dependence will be discussed in more detail and especially compared to measurements in the following.

In Fig. 3 the resulting fractionation as following from (5) and the measurements in the solar wind as shown in Fig. 1 are plotted versus the first ionization potential for the elements listed in Table 1. For chromospheric velocities of 100 m/s and 400 m/s at a density of $N_{\mathrm{H}} = 4\cdot10^{16}\,\mathrm{m}^{-3}$ the theoretical results are matching the measurements in the slow and the fast wind quite well. Please note that here a slightly higher and more realistic density than in Peter (1996) was used. Therefore these results are comparable to the numeric studies in Sect. 5.3.

In the case of the fractionation Mg/O the velocity-dependence is shown in more detail in Fig. 4 for three different chromospheric densities. This shows that the fractionation is vanishing for higher velocities, in which case the transit time through the ionization-diffusion layer is to short for any process to establish a fractionation (see end of Sect. 3). It also shows that the dependence on density is only weak and that sometimes no

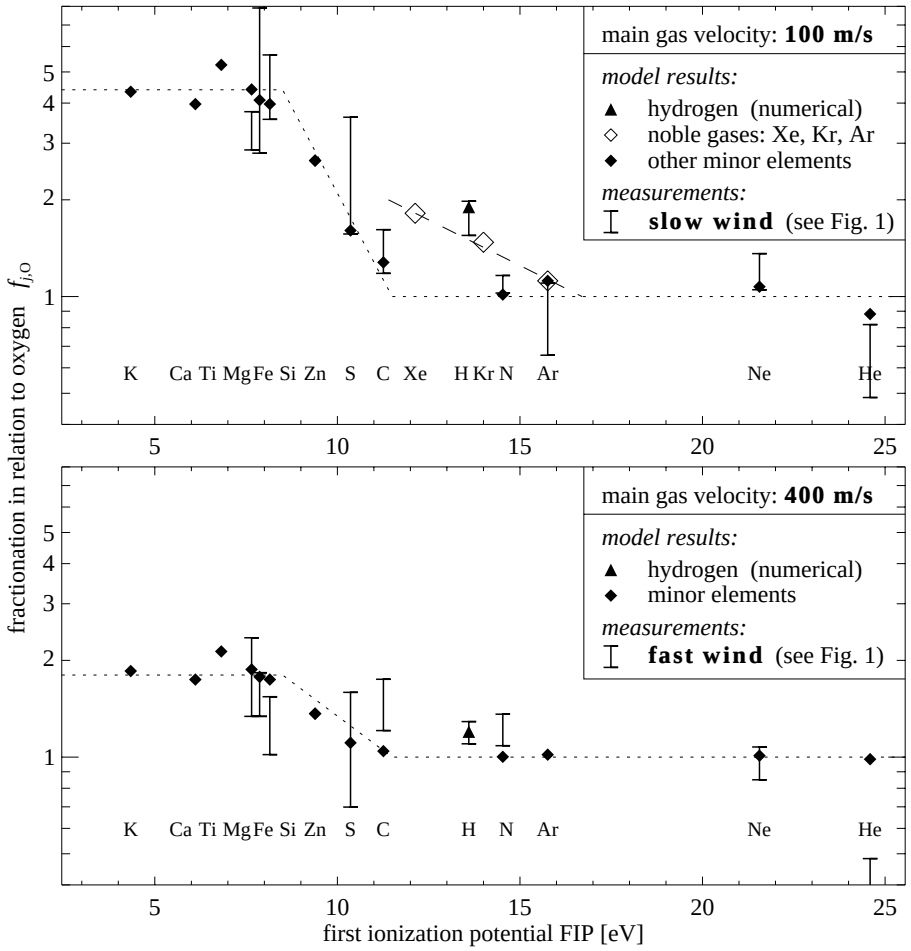

Fig. 3. Calculated fractionation for two different main gas velocities in the chromosphere matching the measurements in the slow and fast wind.
The values for the minors (filled diamonds) and for the noble gases (open diamonds) are calculated from (5) for $N_{\rm H} = 4{\cdot}10^{16}\,{\rm m}^{-3}$ and $T = 10^4$ K. The fractionation of hydrogen (triangles) is taken from the numerical study in Sect. 5.3 (compare the fractionation at the top as given in Fig. 6, left panel). The bars show the respective measurements in the slow and fast wind as shown in Fig. 1. The dotted lines indicate the low- and high-FIP plateaus as shown in Fig. 1, the dashed line the noble gas line. The calculations for the noble gases Xe and Kr are omitted in the 400 m/s case, because no measurements are available for them in the fast wind. Calculations for K, Ca, and Ti are shown to emphasize that the model really results in a low-FIP plateau. The fractionation of oxygen (relative to O) is by definition 1, and for this it is not shown here.

fractionation can be expected in high speed events (compare observations of Bochsler et al. 1996)

To prove this model result it is of interest whether the predicted velocity-dependence can also be found in the measurements in the solar wind. For this in Fig. 5 the relative abundance of Mg/O and the solar wind speed, represented by the α-particle velocity, are shown for one epoch as measured by SWICS/Ulysses (Geiss et al. 1995). Now the relation between the speed and the abundance as derived from these measurements is over-plotted on the theoretical predictions in Fig. 4. According to Anders & Grevesse (1989) the relative abundance in the photosphere is $({\rm Mg/O})_{\rm ph} = 0.045$ (see Table 1). If this value is measured in the solar wind the fractionation is $f_{\rm Mg,O} = 1$.

For $N_{\rm H} = 4{\cdot}10^{16}\,{\rm m}^{-3}$ the curve of the theoretically predicted velocity-dependence of the fractionation is matching the observed data points quite well! Thus, assuming that the velocity structure in the chromosphere can be more or less directly mapped to the solar wind speed, the change of the fractionation with the solar wind speed becomes understandable.

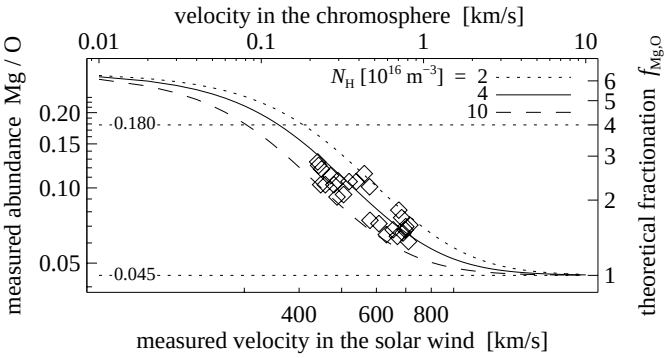

Fig. 4. Velocity-dependence of the fractionation of Mg/O. The three curves show the theoretical dependence of $f_{\rm Mg,O}$ for different densities (upper and right axis). The diamonds show the measured data points from Fig. 5, one for every day of the epoch (lower and left axis).

5.2. Fractionation of the heavy noble gases

As outlined in Sect. 2.3 and Fig. 1 the fractionation of the noble gases (in the slow wind) does not fit into the two plateau structure of the other elements, but forms its own line. In Fig. 3 the theoretical results also for the noble gases as following from (5) are shown.

The three noble gases Xe, Kr and Ar are perfectly on a line, with Xe and Kr clearly enhanced to the high-FIP plateau. But the enhancement is much weaker than indicated by the observations shown in Fig. 1. Nevertheless this discrepancy should not be

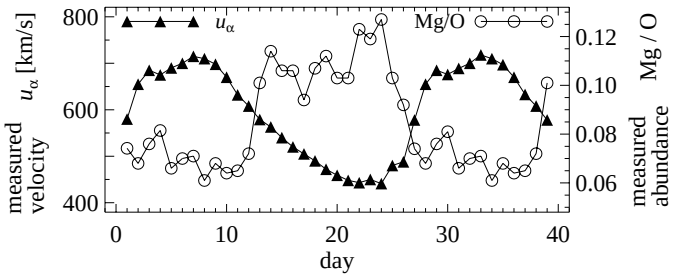

Fig. 5. Solar wind speed and the Mg/O abundance for one epoch as measured by SWICS/Ulysses (from Geiss et al. 1995).

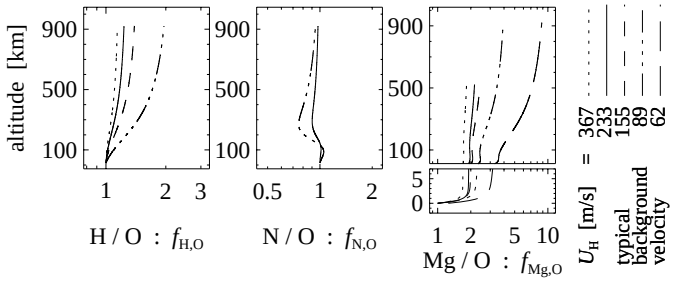

Fig. 6. Absolute fractionation as a function of altitude in the numerical models (Sect. 5.3 and 5.4). The results are plotted for different background models characterized by the typical background velocity.

taken too seriously. The lunar samples from which the noble gas abundances were derived are quite old (Sect. 2.3). As the older ones (some 10^9 years) show a stronger fractionation by 30% than the younger ones (10^8 years) (see Wieler & Baur 1995), one might speculate that the actual fractionation of the noble gases is much weaker than indicated in Fig. 1 and might match the model results in Fig. 3. In every case the qualitative behaviour can be understood by the model.

The special behaviour of the noble gases is reasoned by their atomic properties, mainly their different ionization times. This is analogous to their chemical properties, which are different from the other high-FIPs, too.

5.3. Numerical models: absolute fractionation and hydrogen

To study the variation of the absolute abundances of the elements, e. g. the fractionation of hydrogen to oxygen, a more sophisticated numerical model has to be applied: the density of the trace gases has to be calculated in the background of the main gas. For this purpose (2) and (3) are solved numerically in a given hydrogen-proton background (see the first part of Sect. 4.2 for the boundary conditions).

In the present paper the main gas models of Peter & Marsch (1998) are serving as a background. They have calculated a variety of different hydrogen models which can be characterized by the typical mean velocity (taken at the maximum of the proton density) in the ionization-diffusion layer (see their Sect. 5.3). In their Fig. 3 they show the models with a density at the bottom of 7, 8 and $9{\cdot}10^{16}$ m^{-3} with corresponding typical velocities of 890, 350 and 20 m/s. In the present study main gas models of Peter & Marsch (1998) with typical velocities of 367, 233, 155, 89 and 62 m/s respectively are used (see Fig. 6).

For the main gas models with (typical) velocities of $U_H{\approx}100$ m/s and $U_H{\approx}400$ m/s the fractionation of hydrogen to oxygen turns out to be $f_{\mathrm{H,O}}{\approx}2$ and $f_{\mathrm{H,O}}{\approx}1.2$ respectively at the top of the layer (see Fig. 6, left panel): using main gas models with the typical velocities in the range of those velocities giving the fractionation for the slow and fast wind in the analytical model (Sect. 5.1, Fig. 3), the numerical study gives the measured fractionation of hydrogen to oxygen in the slow and fast wind. (compare Sect. 2.2 and Fig. 3).

At these respective velocities in the numerical models as well the fractionation of the low- to high-FIPs for the slow and fast wind is reproduced; see the example of Mg to O (4 and 2). There is also no fractionation within the high-FIP plateau (N/O); see Fig. 6, middle (N/O) and right (Mg/O) panel, compare with Fig. 3.

In summary these numerical calculations confirm the results of the analytical model, but they can also explain the fractionation of hydrogen to oxygen within a consistent picture. One should note especially that the same (typical) main gas velocities in the numerical calculations and in the analytical model of Sect. 5.1 lead to the same fractionation. Thus all the effects included additionally in the numerical model, mainly gravitation and recombination, do not play an important role for the fractionation.

5.4. Polar plumes

In the analytical study the fractionation of magnesium can only reach a maximum value of about 6 (see Fig. 4). In contrast to this in the numerical model a much stronger fractionation can be found: for very low mean background velocities of only ≈50 m/s the fractionation Mg/O can reach a factor of 10 (see right panel of Fig. 6).

This corresponds well to the observations in polar plumes, e. g. by Widing & Feldman (1992) or Sheeley (1996), who found strong Mg/O fractionations of up to 10 or even 15. For this they conclude that the plumes cannot contribute a significant fraction to the solar wind mass flux, because of the different abundances. Thus the plumes have to be quasi-static, which means that the velocities in the chromosphere of the plumes are indeed very low.

Thus their results for the plumes, namely low velocity and strong fractionation, can be understood (also quantitatively) with the presented fractionation model.

6. Absolute and relative velocities: the role of diffusion

6.1. Absolute velocities

The profiles of the absolute velocities of the neutrals are relatively flat. As can be seen in the example of oxygen (Fig. 7, right panel), the gradients of the scaled velocity at the bottom and the top of the layer are small, while a noticeable change can only be found inbetween, in the region where the material gets

ionized (go back to end of Sect. 4.2 for an explanation of what "scaled" means).

This compares well with the (simpler) model of Marsch et al. (1995) who found the velocity of the neutrals to be constant (see their Figs. 3 and 4). This result is of great importance for the analytical model of Peter (1996) and the analytical studies in the present paper (see second part of Sect. 4.2).

As pointed out in Sect. 5.1 after Eq. (4) in the analytical model *all* the trace gases have higher velocities at the bottom than the background. This at first seemingly strange behaviour is revised somewhat in the numerical models.

In the numerical models the high-FIP elements are entering the layer with smaller velocities than the main gas (see Fig. 7, left and middle panel for the example of oxygen). But still, the low-FIPs are somewhat faster at the bottom than the background (not shown). How can this be understood?

Fist one has to note that in a one-dimensional diffusive model this behaviour has to be expected, because the observations tell that e.g. magnesium is enriched in relation to hydrogen (Sect. 2 and Fig. 1). The only way to do that in a model like this is to have a higher velocity of Mg than of hydrogen at the bottom, compare (9) below.

Marsch et al. (1995) discussed in their Sect. 3 a pure diffusion model. In a static situation an enrichment of e.g. Mg to hydrogen can be achieved by a "climbing up" of Mg-ions (see their Fig. 2): the net effect will be a (small) upward velocity of Mg, even though the main gas has zero velocity. The fractionation results from the different ability of the different species to climb up – some might even fall down. In a situation where the main gas is flowing up, this means that some species might be even (a bit) faster than the main gas, which explains the above problem. This is simply a result of the diffusion.

6.2. Relative velocities

Diffusion, i.e. the fact that the different elements have different velocities, plays a crucial role in the presented model. Fractionation as defined in (1) can also be expressed in terms of the velocities at the bottom of the ionization-diffusion layer by using the definition of the total particle flux of an element j, $\Phi_j = N_j\, U_j$, as given by the total density N_j and the mean velocity U_j of the respective element.

$$f_{j,k} \;=\; \frac{(N_j/N_k)^{\rm t}}{(N_j/N_k)^{\rm b}} \;=\; \frac{\Phi_j^{\rm t}}{\Phi_j^{\rm b}}\,\frac{\Phi_k^{\rm b}}{\Phi_k^{\rm t}}\,\frac{U_k^{\rm t}}{U_j^{\rm t}}\,\frac{U_j^{\rm b}}{U_k^{\rm b}}, \tag{8}$$

where the indices $^{\rm t}$ and $^{\rm b}$ indicate the respective values to be taken at the top and the bottom of the layer.

Because of the conservation of flux (2) the total particle flux of an element at the bottom has to be the same as at the top, $\Phi_j^{\rm t}/\Phi_j^{\rm b} = 1$. Additionally at the top of the layer the effective Coulomb-collisions lead to equal velocities, $U_k^{\rm t}/U_j^{\rm t} = 1$ of the different elements, which are ionized there. For this by definition the fractionation (8) is given by the quotient of the respective velocities (in the neutral phase) at the bottom,

$$f_{j,k} \;=\; U_j^{\rm b} \,/\, U_k^{\rm b}. \tag{9}$$

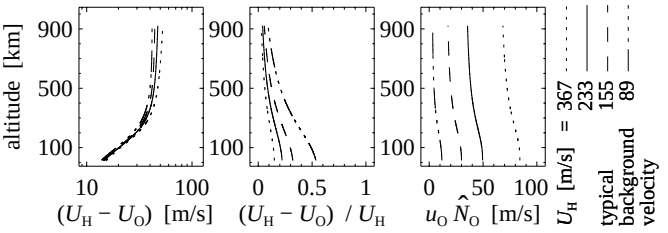

Fig. 7. Relative *mean* velocity of oxygen to hydrogen (left and middle) and scaled *absolute* velocity of oxygen (right) in a hydrogen background following the numerical model discussed in Sect. 5.3 for four different background models.
The uppercase $U_{\rm H}$ and $U_{\rm O}$ denote the mean velocity of the neutral and ionized components of hydrogen and oxygen, while the lowercase $u_{\rm O}$ denotes the velocity of neutral oxygen. (See Sect. 6.2 for the left and middle panel, second part of Sect. 4.2 and 6.1 for a discussion of the right panel.)

Thus to calculate the fractionation one has to determine the diffusive equilibrium at the bottom of the ionization-diffusion layer.

One idea that might arise is the following: as the ionization layer is thin compared with the gravity scale height in the chromosphere, the medium has to be homogeneous at the bottom. In this case one *assumes*, that "far away", i.e. some ionization lengths from the ionization-diffusion layer, no diffusion can occur. Following (9) this would mean that fractionation is excluded.

But in a more general case, if homogeneity is *not* taken for granted and the diffusive equilibrium is calculated, it turns out that even at a distance of some ionization lengths a small but not-vanishing diffusion occurs! These (diffusion) velocities are small, but as the quotient of the velocities determines the fractionation, the latter one can be relatively large.

In Fig. 7 some aspects of the diffusion as following from the numerical models as discussed in Sect. 5.3 are shown for the example of oxygen in a hydrogen background. In the left panel it can be seen that the absolute value of the diffusion velocity $(U_{\rm H} - U_{\rm O})$ is small. At the bottom it is of the order of only 10 m/s. In the ionized phase a diffusive equilibrium is reached, were the diffusion velocity is finite (40 m/s) but small compared to the background speed, which can be of the order of some km/s. This finite diffusion velocity might be compared to the observed difference speeds in the solar wind of the order of some 10 km/s (Grünwald 1996).

But if the diffusion velocity is compared to the hydrogen velocity (middle panel, $(U_{\rm H} - U_{\rm O})/U_{\rm H}$) it turns out that in deed at the top the velocities are nearly equal, while at the bottom, i.e. in the neutral phase, the velocities can differ significantly, e.g. in the case of O and H up to 50%.

The conclusion from this must be that one cannot simply assume homogeneity at the bottom and thus rule out the fractionation. On the contrary, one has to calculate the diffusive equilibrium properly. No diffusion is a good assumption at the top in the ionized phase, where the very effective Coulomb-collisions are of importance (see Table 2 for a comparison of

the different collisional rates). But at the bottom in the neutral phase the low efficiency of the neutral-neutral and neutral-ion collisions enables a small but not-vanishing diffusion, leading to a significant fractionation.

7. Conclusions

On the basis of the fractionation mechanism proposed by Marsch et al. (1995) a more sophisticated model for the ion-neutral separation was presented, which explains the observed abundance anomalies for a large variety of phenomena. The mechanism is based on properties dominated by atomic parameters, mainly on photoionization time and diffusion: the newly ionized particles are trapped within the wind, which causes the low-FIPs to be enriched compared to the high-FIPs. The diffusion in the neutral phase additionally regulates the fluxes of the different species. But also the velocity has an influence: in the case of a higher speed the fractionation has less time to act and thus the fractionation is weaker. Because the mechanism is mainly based on atomic properties it is not restricted to a special geometry, e. g. of the magnetic field.

This gives the possibility to apply the results presented here for the solar corona and wind also to (cool) stars. As long as the respective star is not too hot and thus somewhere in the stellar atmosphere a layer is existing, where the material is neutral and gets ionized when leaving the stellar surface into the wind, the presented model should apply. Thus e. g. the absence of the fractionation in the corona of Procyon (Drake et al. 1995) may be simply explained by a wind with high velocities in its source region. But for a proper application of the presented model to stars first of all the ionization times of the various elements have to be calculated from the respective stellar spectra.

It should be noted that the fractionation of helium cannot be understood within a purely chromospheric ionization-diffusion model (see Peter & Marsch 1998). Helium has to be described in a chromosphere-corona model as done by Hansteen et al. (1997).

As in other fractionation models before, this model gives a two-plateau structure of the fractionation as a function of the first ionization potential. But with the help of the presented analysis for the first time it is possible to understand the fractionation in a great variety of phenomena in a quantitative way:

- The fractionation in the slow *and* the fast wind can be understood with the theoretically predicted velocity-dependence of the fractionation matching the observations.
- A comparison of the theoretical fractionation in the chromosphere with the measured one in the solar wind leads to chromospheric velocities of 100 km/s and 400 km/s in the slow and fast wind respectively.
- With the help of the velocity-dependence it can be explained why sometimes in high speed streams in the wind no fractionation is found.
- The fractionation of the heavy noble gases as measured in lunar regolith can be understood (in a qualitative way).
- The numerical studies enable a determination of the absolute fractionation, i. e. the fractionation in relation to hydrogen: the position of H in the fractionation pattern fits well with the in-situ measurements in the slow and fast wind.
- The very strong fractionation as found in polar plumes can be modeled by assuming the plumes to be quasi-static as suggested by some measurements.

To explain all these different fractionation related phenomena within only *one* model, based on the well known processes of photoionization and diffusion, is the major achievement of the presented paper.

Acknowledgements. I feel grateful to Eckart Marsch because of the many ingenious and helpful discussions we had. Special thanks are due to Roland Bodmer, who had the basic idea for the vivid bathing tub analogy. Sincere thanks are due to J.-C. Hénoux for his helpful comments on this paper.

References

Anders E., Grevesse N., 1989, Geochim. Geocosm. Acta 53, 197
Arnaud M., Rothenflug R., 1985, A&A 60, 425
Bochsler P., Bodmer R., Kern O., et al., 1996, Eos Trans. AGU 77, (17)S210 (abstract)
Cargill P.J., Priest E.R., 1980, Solar Physics 65, 251
Cook J.W., Cheng C.-C., Jacobs V.L., Antiochos S.K., 1989, ApJ 338, 1176
Drake J.J., Laming J.M., Widing K.G., 1995, ApJ 443, 393
Drake J.J., Laming J.M., Widing K.G., 1996, ApJ 462, 948
Drake J.J., Laming J.M., Widing K.G., 1997, ApJ 478, 403
Geiss J., Gloeckler G., von Steiger R., 1995, Space Sci. Rev. 72, 49
Grünwald H., 1996, In: Proceedings of the CELIAS Science Workshop 1996 held in Seeon, Germany
Hansteen V.H., Leer E., Holzer T.E., 1997, ApJ 482, 498
Hénoux J.-C., 1995, Adv. Space Res. 15, (7)23
Hénoux J.-C., Somov B.V., 1992, First Ionization Potential Fractionation. In: Coronal Streamers, Coronal Loops and Coronal and Solar Wind Composition. ESA SP-348, p. 325
Hirschberg J., Alksene A., Colburn D.S., Bame S.J., Hundhausen A.J., 1970, J. Geophys. Res. 75, 1
Klimchuk J.A., Mariska J.T., 1988, ApJ, 328, 334
Landini M., Monsignori Fossi B.C., 1990, A&AS 82, 229
Lotz W., 1967, ApJS 14, 207
Marsch E., von Steiger R., Bochsler P., 1995, A&A 301, 261
Meyer J.-P., 1993, Element Fractionation at Work in the Solar Atmosphere. In: Prantzos N., Vangioni-Flam E., Cassé M. (eds.) Origin and Evolution of the Elements. Cambridge Univ. Press, p. 26
Meyer J.-P., 1996, Abundance Anomalies in the Solar Outer Atmosphere. In: Trân Thanh Vân J., Celnikier L., Trung H.C., Vauclair S. (eds.) The Sun and Beyond. Editions Frontières, Gif-sur-Yvette, p. 27
Peter H., 1996, A&A 312, L37
Peter H., Marsch E., 1998, A&A 333, 1069
Pottasch S.R., 1963, ApJ 137, 945
Raymond J.C., Kohl J.L., Nocci G., et al., 1997, Solar Physics, 175, 645
Schunk R.W., 1975, Planet. Space Sci. 23, 437
Sheeley N.R. Jr., 1996, ApJ 469, 423
Sheeley N.R. Jr., Wang Y.-M., Hawley S.H., et al., 1997, ApJ 484, 472
Vauclair S., 1996, A&A 308, 228
Vernazza J.E., Avrett E.H., Loeser R., 1981, ApJS 45, 635
von Steiger R., Geiss J., 1989, A&A 225, 222

von Steiger R., Wimmer Schweingruber R.F., Geiss J., Gloeckler G., 1995, Adv. Space Res. 15, (7)3
von Steiger R., Geiss J., Gloeckler G., 1997, Composition of the Solar Wind. In: Jokipii J.R., Sonett C.P., Giampapa M.S. (eds.) Cosmic Winds and the Heliosphere. Univ. of Arizona Press, Tucson, p. 581
Widing K.G., Feldman U., 1992, ApJ 392, 715
Wieler R., Baur H., 1995, ApJ 453, 987